


ORIGINAL ARTICLE

Open Access



Evaluation of Surface Roughness of Aluminum Alloy in Burnishing Process Based on Chaos Theory

Zhipeng Yuan^{1,2}, Zhenyu Zhou^{1,2}, Zhiguo Jiang^{1,2}, Zeyu Zhao^{1,2}, Cong Ding^{1,2*} and Zhongyu Piao^{1,2*} 

Abstract

Burnishing experiments with different burnishing parameters were performed on a computer numerical control milling machine to characterize the surface roughness of an aluminum alloy during burnishing. The chaos theory was employed to investigate the nonlinear features of the burnishing system. The experimental results show that the power spectrum is broadband and continuous, and the Lyapunov exponent λ is positive, proving that burnishing has chaotic characteristics. The chaotic characteristic parameter, the correlation dimension D , is sensitive to the time behavior of the system and is used to establish the corresponding relationship with the surface roughness. The correlation dimension was the largest, when the surface roughness was the smallest. Furthermore, when the correlation dimension curve decreases, the roughness curve increases. The correlation dimension and surface roughness exhibit opposite variation trends. The higher the correlation dimension, the lower the surface roughness. The surface roughness of the aluminum alloy can be characterized online by calculating the correlation dimension during burnishing.

Keywords Aluminum alloy burnishing, Power spectrum, Correlation dimension, Lyapunov exponent, Surface roughness

1 Introduction

Aluminum alloy is widely used in ships, railways, transportation, aerospace, and other fields because of its high specific strength, strong corrosion resistance, and light weight [1, 2]. Most failures of aluminum alloys occur on the surface in service [3, 4]. Enhancing the comprehensive protection ability of aluminum alloy surfaces through surface nanocrystallization can significantly improve the service performance and life of the material [5–7].

In recent years, the development of metal surface nanocrystallization techniques has diversified, and various processing methods have been proposed for surface nanocrystallization. Zhu et al. investigated the effect of ultrasonic shot-peening on the surface structure, hardness, and corrosion resistance of 7075 aluminum alloy. The results showed that the surface hardness and roughness increased with increasing shot-peening time. When the shot-peening duration exceeded a specific level, the rate of increase decreased and then reached a stable value. The maximum surface hardness determined during the test was 249.6 HV and 46% higher than that of the original sample [8]. Gao et al. examined the effect of a surface mechanical grinding treatment on the fatigue properties of 7075T6 aluminum alloy. The results indicated that within a particular range of impact strength, surface mechanical grinding could increase the fatigue strength of the material. The near-surface microhardness increased with increasing surface mechanical grinding strength and surface

*Correspondence:

Cong Ding
dingcong68@zjut.edu.cn;
Zhongyu Piao
piaozhy@zjut.edu.cn

¹ College of Mechanical Engineering, Zhejiang University of Technology, Hangzhou 310012, Zhejiang, China

² Key Laboratory of Special Purpose Equipment and Advanced Processing Technology, Ministry of Education and Zhejiang Province, Zhejiang University of Technology, Hangzhou 310012, China



© The Author(s) 2023. **Open Access** This article is licensed under a Creative Commons Attribution 4.0 International License, which permits use, sharing, adaptation, distribution and reproduction in any medium or format, as long as you give appropriate credit to the original author(s) and the source, provide a link to the Creative Commons licence, and indicate if changes were made. The images or other third party material in this article are included in the article's Creative Commons licence, unless indicated otherwise in a credit line to the material. If material is not included in the article's Creative Commons licence and your intended use is not permitted by statutory regulation or exceeds the permitted use, you will need to obtain permission directly from the copyright holder. To view a copy of this licence, visit <http://creativecommons.org/licenses/by/4.0/>.

roughness [9]. He et al. evaluated the surface properties of an aircraft 5A06 aluminum alloy using laser shock peening. They found that laser shock peening increased the microhardness of the material by 65% and ultimate tensile strength by 27% [10]. Generally, surface nanocrystallization techniques, such as ultrasonic shot peening, surface mechanical grinding, and laser shock peening, significantly improve the hardness, fatigue strength, and tensile strength of metals [11–13]. However, problems, such as insufficient attention to surface roughness and little improvement, still exist. In engineering applications, such as surface strengthening of aircraft fuselages, which require high surface roughness, secondary processing is often required to improve the surface roughness of materials. This undoubtedly increases processing costs [14].

Burnishing is a surface nanocrystallization technique, with positive effects on the hardness, wear resistance, and surface roughness of metals [15–17]. Good surface roughness improves the resistance of metals to wear, corrosion, and fatigue [18–20]. In this study, burnishing processing parameters of the optimum surface roughness was investigated using the orthogonal experiment method. Burnishing is a dynamic process in which the system parameters and state variables function jointly. Its essence is a highly complex nonlinear process that requires investigation using nonlinear scientific methods. Surface roughness was gradually generated using the tool feed during burnishing. This parameter is a state variable, and can be used to characterize the evolution of system behaviors. Surface roughness is typically measured off-line after burnishing. This measurement makes it difficult to reflect the variation in burnishing process features in real time. In this study, the nonlinear characteristics of the friction coefficient during the burnishing process were analyzed based on the chaos theory to solve this problem. Moreover, the relationship between the chaotic characteristics and surface roughness was further established, providing a theoretical basis for online surface roughness measurements. The chaos theory is also called nonlinear dynamics, which is widely used for determining the nonlinear features of univariate time series. In the chaotic method, the nonlinear features of a system are characterized based on the unique performance of the characteristic parameters. The traditional characteristic parameters are the Lyapunov exponent λ and correlation dimension D . The Lyapunov exponent λ is used to analyze the chaotic characteristics of the system,

and the correlation dimension D is used to characterize the dynamic changes in the system state with time [21].

In this study, nine groups of burnishing process tests were designed using the orthogonal test method, and the burnishing friction coefficient signal and surface roughness of each test group were collected. Based on the orthogonal analysis method, the experimental parameters were determined to obtain the best surface roughness, and the tenth group of tests was performed. The power spectrum method and the Lyapunov exponent method were used to verify the chaotic characteristics of the burnishing process, and the correlation dimension was used to obtain the correlation with the surface roughness. The corresponding relationship was verified using the test results of the tenth experimental group.

2 Experiments

2.1 Experimental Materials and Equipment

The experimental material was annealed 7075-T6 aluminum alloy. Its main components are listed in Table 1. Each sample was a rectangular plate of 65 mm \times 30 mm \times 10 mm. During the entire burnishing process, the burnishing tool rotated and translated to the sample surface for processing, exhibiting a spiral feed, as shown in Figure 1(a). The burnishing zone with an area of 60 mm \times 26 mm was divided into two parts: one burnished once (Zone A), and the other burnished twice (Zone B), as shown in Figure 1(b). Zone B, with an area of 10 mm \times 26 mm, was the main research object, where Areas 1, 2, and 3 represent the areas of the roughness measurements. Before burnishing, the samples were pre-processed using a grinding machine to ensure the

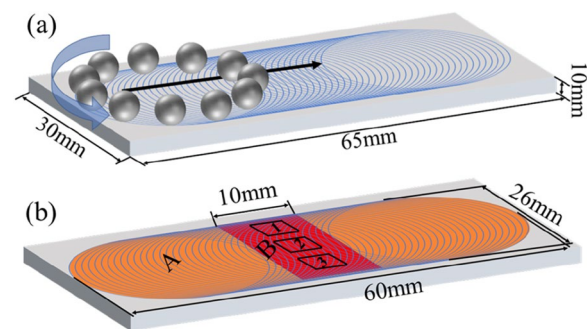


Figure 1 Burnishing process: (a) Burnishing path, (b) Burnishing area

Table 1 Constituents of 7075-T6 aluminum

Chemical element	Si	Fe	Cu	Zn	Ti	Mn	Mg	Cr	Al
Content (Wt%)	0.36	0.42	1.58	5.8	0.11	0.17	2.45	0.225	Bal.

good flatness of each sample surface. The sample surface was then rinsed with alcohol to remove the surface dust and other attached particles. A six-axis Kistler force sensor was used to measure the burnishing force. The main performance indices of the force sensor were sensitivity of 6 mV/V, the linearity of 7% F.S, and hysteresis of 5% F.S. During burnishing, lubricating oil was continuously added onto the sample surface, to lubricate and remove the metal particles or debris generated from the adhering burnishing process. The lubricating oil was No.10 A-grade sewing machine oil, with a kinematic viscosity (40 °C) of 6 mm²/s, a flashpoint (opening) of 140 °C, and a pour point of − 5 °C.

The experimental equipment (Figure 2) consisted of a plane burnishing tool, sample fixed platform, Kistler force sensor, charge amplifier, and data collector. The head of the burnishing tool was attached with 11 burnishing balls distributed along the circumference to improve the burnishing efficiency and expand the processing area. The burnishing balls consisted of GCr15, and their diameter, hardness, and yield strength were 10 mm, 63HRC, and 518 MPa, respectively. The burnishing tool was installed on the spindle box of the XK-714 computer numerical control milling machine using clamps, and the spindle rotated to drive the rotation of the burnishing tool. The Kistler force sensor was mounted on the machining platform of the milling machine using bolts, and the sample-fixing platform was mounted on the Kistler force sensor using bolts. During testing, the normal force was directly applied to the sample surface and transmitted to the Kistler force sensor through a sample-fixing platform. The analog signals in the x -, y -, and z -directions during burnishing were measured using the Kistler force sensor. Next, the analog signals were amplified using the charge amplifier, converted into discrete digital signals by an A/D converter in the data collector, and stored in a computer as data files.

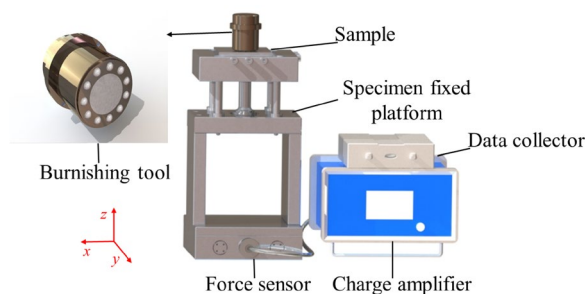


Figure 2 Schematic of burnishing device

Table 2 Orthogonal tests

Test	Burnishing depth (mm)	Spindle speed (r/min)	Feed rate (mm/min)
1	0.12	3000	70
2	0.12	2000	40
3	0.12	1000	10
4	0.09	3000	40
5	0.09	2000	10
6	0.09	1000	70
7	0.06	3000	10
8	0.06	2000	70
9	0.06	1000	40

2.2 Orthogonal Test Method

In this study, the effects of the burnishing depth, spindle speed, and feed rate on the system behavior were analyzed. The specific test scheme for the orthogonal tests is presented in Table 2.

3 Results

3.1 Friction Coefficient

The machined lengths of the samples during the tests were equal, and the feed rates of the tools in the machined direction and the machined durations were different. Therefore, the test was performed using the equidistant sampling method to ensure the comparability of the experimental data. The feed distance of the burnishing tool in the test was 35 mm, and the number of sampling points was 21000; thus, the sampling distance was 1/600 mm. The first 20000 data points were used in this study. The sampling frequency value was determined experimentally according to the feed rate of the burnishing tool, specifically $f/v = 10$, where f is the sampling frequency, and v is the feed rate of the burnishing tool. The

Table 3 Orthogonal parameters

Test	Processing time (s)	Sampling frequency f (Hz)
1	30	700
2	52.5	400
3	210	100
4	52.5	400
5	210	100
6	30	700
7	210	100
8	30	700
9	52.5	400

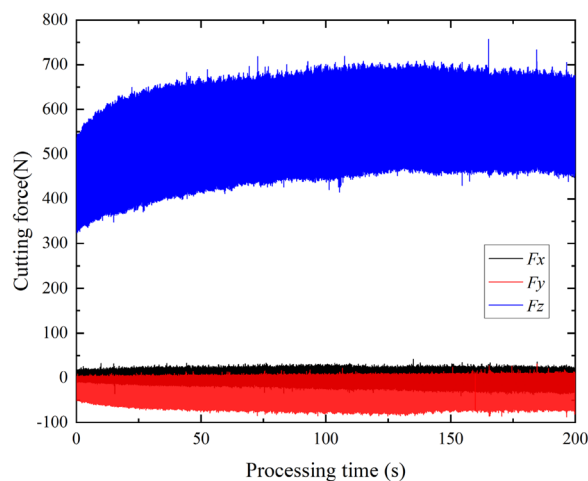


Figure 3 Time series of force signals of F_x , F_y , and F_z extracted in Test 5

values of the processing time t and sampling frequency f for the different test parameters are listed in Table 3. By taking Test 5 as an example, the forces along the x -, y -, and z -axes in each test are denoted F_x , F_y , and F_z , respectively, as shown in Figure 3, where the shadow between F_x and F_y represents the overlapping part. It is evident that the local fluctuation of the three forces is significant; however, the fluctuation of the forces is relatively stable. The burnishing friction coefficient was calculated as follows to comprehensively reflect the correlation between the force and system behaviors during burnishing:

$$\mu = \frac{\sqrt{F_x^2 + F_y^2}}{F_z}, \quad (1)$$

where μ is the burnishing friction coefficient.

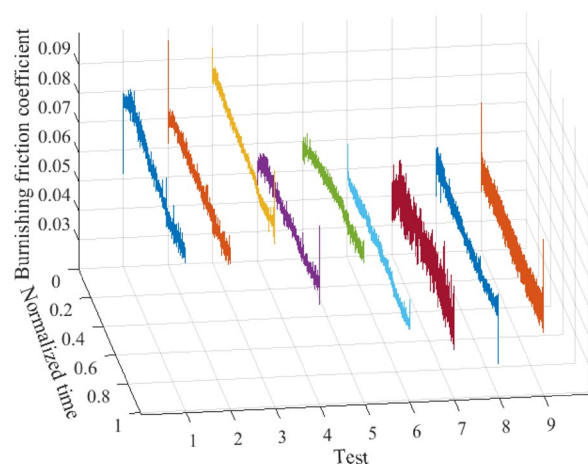


Figure 4 Burnishing friction coefficients in Tests 1–9

Consequently, the time series of the friction coefficient was denoised. The wavelet method with db4_level8 was adopted, and the denoised signals of all the tests are shown in Figure 4. The burnishing friction coefficient was influenced by the burnishing depth. For Tests 7, 8, and 9, the burnishing depth was 0.06 mm, and the amplitude of the burnishing friction coefficient ranged between 0.4 and 0.5. For Tests 4, 5, and 6, the burnishing depth was 0.09 mm, and the amplitude of the burnishing friction coefficient was between 0.05 and 0.06. For Tests 1, 2, and 3, the burnishing depth was 0.12 mm, and the magnitude of the burnishing friction coefficient was 0.07–0.09. When the depressing amount was 0.06 mm, the signal fluctuated significantly. The main reason for this is the shallow burnishing depth, and the contact between the main shaft of the machine tool and the sample is insufficient. When a sample is processed, the inherent vibration of the machine tool is transmitted to the sample, generating a significant fluctuation in the burnishing friction coefficient signal. As the depression depth increases, the signal fluctuations smoothen.

3.2 Surface Roughness

An Olympus OLS4000 laser scanning confocal microscope with a measurement range of $259 \mu\text{m} \times 259 \mu\text{m}$ was used to characterize the burnished sample surfaces. The device had an ultra-high level ($0.12 \mu\text{m}$ and a z -axis resolution of $0.01 \mu\text{m}$). For the burnished samples, three measurement points were selected in Zone B, as shown in Figure 1(a), and the average value was used as the evaluation index to determine the corresponding surface roughness.

The surface roughness values for the aluminum alloy samples after burnishing in all the tests are listed in Table 4. The surface roughness value of the Test 3 sample was the highest, and that of the Test 8 sample was the lowest. Significantly, the surface roughness values of all the burnished samples were significantly lower than

Table 4 Surface roughness values for Test 1–9

Test	Original surface roughness S_q (nm)	Burnishing surface roughness S_q (nm)
1	958	205
2	797	297
3	919	319
4	844	151
5	853	156
6	838	133
7	974	131
8	897	78
9	786	92

those of the original samples, indicating that the burnishing technique can improve the surface roughness. Moreover, the surface roughness ranges were 200–300, 130–150, and 70–130 nm at burnishing depths of 0.12, 0.09, and 0.06 mm, respectively. This phenomenon indicates that burnishing depth has the most significant influence on surface quality. Test 1, 5, and 9 are taken as examples because their test parameters include the full range of the burnishing depth. The three-dimensional topographies of Tests 1, 5, and 9 samples and the original sample are depicted in Figure 5. The difference in the feature distribution can be determined by observing the color of the sample surface and the color scale. The original sample had the worst surface smoothness, with an evident streak texture and poor uniformity. The surface smoothness values of Tests 1, 5, and 9 improved significantly compared to that of the original samples, the streak texture reduced, and the surface was relatively flat. Test 9 had the best surface smoothness, followed by Test 5, and finally, Test 1. This is because burnishing causes plastic flow on the surface of the samples, the surface roughness peaks plastically and flows to fill the valleys, and the surface tends to

be flat. An increase in the burnishing depth can cause slight chipping on the microscopic surface of the sample, but the surface smoothness is still more significant than that of the original specimen surface.

4 Discussion

4.1 Effect of Burnishing Parameters on Surface Roughness

The surface roughness value in Test 8 was the lowest, and the surface smoothness was the best, when the burnishing depth, spindle speed, and feed rate were 0.06 mm, 2000 r/min, and 40 mm/min, respectively (Table 4). However, this is not necessarily the best combination of the three factors and the three levels in Table 4. Hence, the best surface smoothness was obtained to determine the best combination. The relationships between the burnishing depth and the average roughness, the spindle speed and the average roughness, and the feed rate, and the average roughness were plotted (Figure 6). When the burnishing depth, spindle speed, and feed rate values were 0.06 mm, 3000, and 70 mm/min, respectively, the average surface roughness was the lowest. This group of parameters was defined as Test 10 of the burnishing test. The measured surface roughness value was 72 nm,

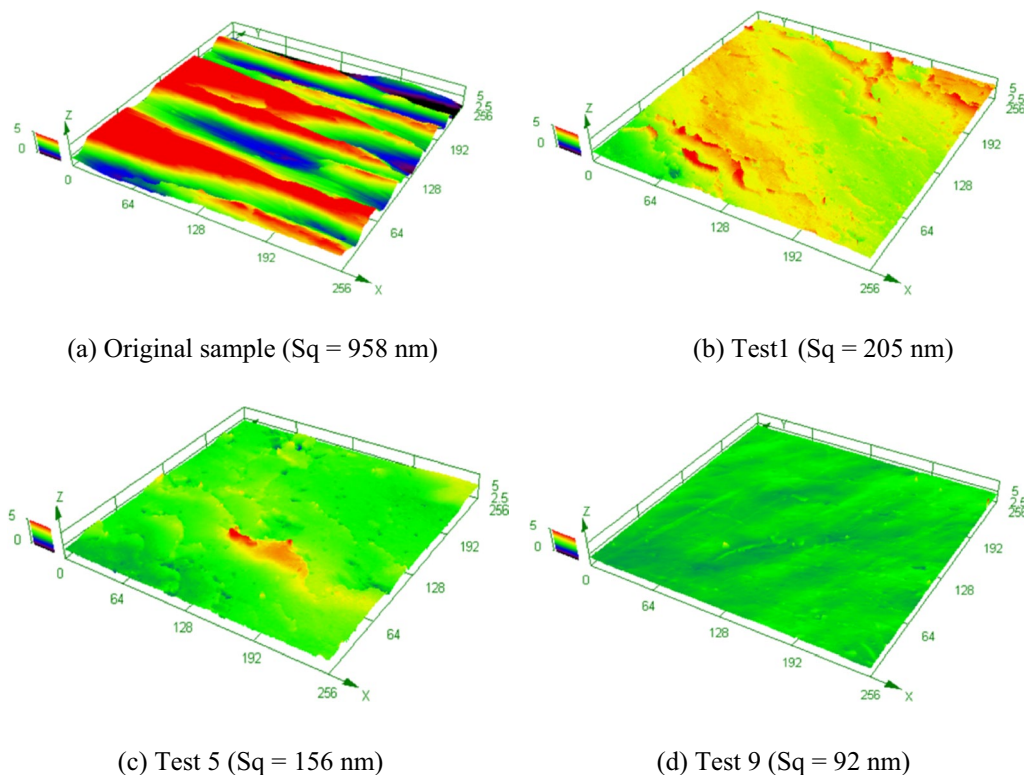


Figure 5 Three-dimensional topography: (a) Original sample, (b) Test 1 (burnishing depth is 0.12 mm, spindle speed is 3000 mm, and feed rate is 70 r/min), (c) Test 5 (burnishing depth is 0.09 mm, spindle speed is 2000 mm, and feed rate is 10 r/min), (d) Test 9 (burnishing depth is 0.06 mm, spindle speed is 1000 mm, and feed rate is 10 r/min)

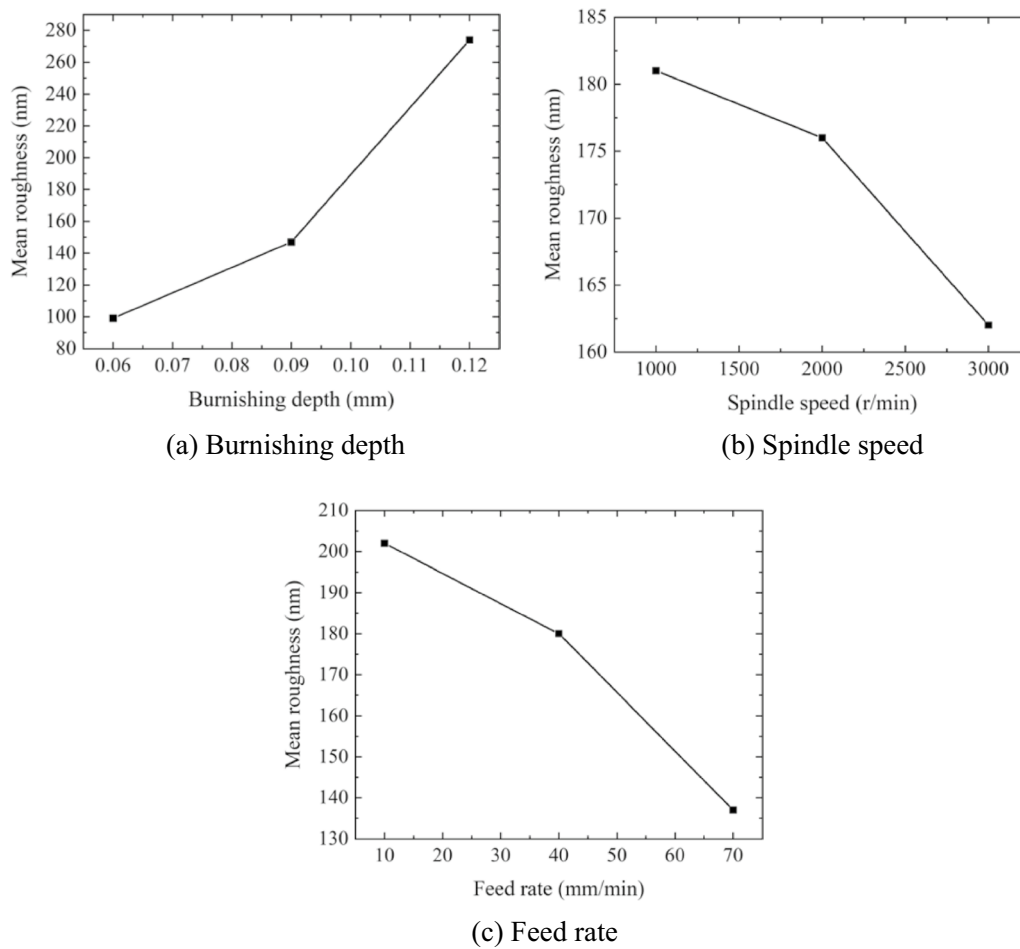


Figure 6 Relationships between machining parameters and average roughness: (a) Burnishing depth and average roughness, (b) Spindle speed and average roughness, (c) Feed rate and average roughness

lower than the best surface roughness values in Table 4. The surface roughness in Test 10 was considered the best surface roughness.

Furthermore, the degree of influence of different burnishing parameters on surface roughness was assessed. The most significant factors influencing the surface roughness were determined through range analysis. The most significant influencing factor for the surface roughness of the sample during burnishing is the burnishing depth, followed by the feed rate, and finally, the spindle speed (Figure 7).

4.2 Chaotic Characteristics of Friction Coefficient

Burnishing is a complex nonlinear process, in which various disciplines, such as mechanics and material

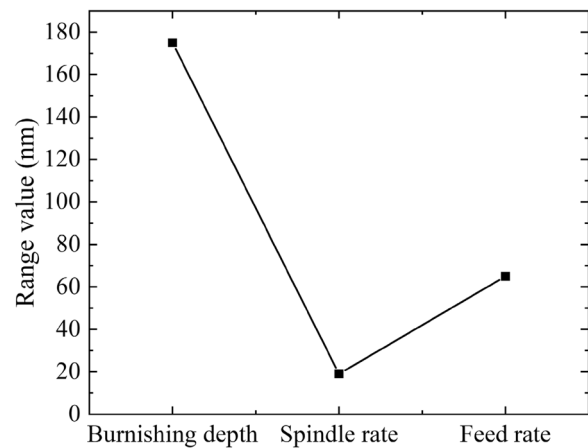


Figure 7 Range analysis

science, are combined. Nonlinear factors, such as surface roughness and section hardness change significantly at a specific burnishing depth, spindle speed, and feed rate. This indicates that burnishing has chaotic characteristics that reveal a burnishing system, and help in conducting on-line research on variations in surface roughness with processing parameters during burnishing.

4.2.1 Qualitative Analysis Using Power Spectrum Method

The power spectra of periodic and quasi-periodic signals are discrete and consist of fundamental frequencies and harmonics of various orders. The chaotic signal, owing to its internal nonlinear action, causes the evolutionary of the system to be stochastic; therefore, its power spectrum is broadband and continuous [22]. This phenomenon can be verified using the logistic mapping system, and its formula is expressed as follows:

$$x_{n+1} = ux_n(1 - x_n), \mu \in [0, 4], x_n \in [0, 1]. \quad (2)$$

The state of the logistic system changes with the variable u ; at $u = 3.571$, the system reaches a periodic state, and at $u = 3.9$, the system enters a chaotic state. The power spectra are shown in Figure 8. Figure 8(a) shows a power spectrum diagram of a periodic system. Here, the frequency corresponding to the tip protrusion parts is the fundamental frequency, and the frequency corresponding to the gentle parts is the harmonics, an integer multiple of the fundamental frequency. Figure 8(b) shows a power spectrum diagram of a chaotic system. In this case, the power spectrum exhibits broadband, and continuous characteristics, and has no peaks.

Figure 9 shows the power spectral densities of the burnishing coefficient friction for Tests 1–9. The power spectra were broadband and continuous, and the trend of the power spectrum first decayed rapidly and then stabilized. This phenomenon implies that the burnishing

friction coefficient exhibits nonlinear characteristics and induces stochastic evolution behaviors in the burnishing system. This is an inherent characteristic of chaotic systems. Some noise signals were mixed in the friction coefficient signal owing to the vibration of the machine during the burnishing process. Therefore, when the normalized frequency is 0.18, 0.3, or 0.69 rad/ π , the power spectrum will have small peaks.

4.2.2 Quantitative Analysis Using Maximum Lyapunov Exponent Method

The friction coefficient extracted from the burnishing system, univariate time series $X = \{x_1, x_2, x_3, \dots, x_n\}$, contains important system behavior information. It is necessary to extend the friction coefficient to a high-dimensional phase space to reflect the dynamic characteristics of the burnishing system. According to Takens theorem [23], the phase space reconstruction of the time series of the friction coefficient is performed, and the reconstruction matrix is expressed as follows:

$$Y = \begin{bmatrix} Y_1 \\ Y_2 \\ \vdots \\ Y_N \end{bmatrix} = \begin{bmatrix} x_1 x_{1+\tau} \cdots x_{1+(m-1)\tau} \\ x_2 x_{2+\tau} \cdots x_{2+(m-1)\tau} \\ \vdots \\ x_N x_{N+\tau} \cdots x_{N+(m-1)\tau} \end{bmatrix}, \quad (3)$$

where $N = n - (m-1)\tau$ and is the number of vectors Y_p and n is the number of data points x_i ; τ is the time delay calculated using the mutual information method [24], as expressed by Eq. (4), and m is the optimal embedding dimension calculated using the false nearest neighbors method [25], the formula is given as Eq. (5):

$$I(X, Y) = \sum_i \sum_j P_{xy}(x_i, y_i) \log_2 \left[\frac{P_{xy}(x_i, y_i)}{P_x(x_i)P_y(y_i)} \right], \quad (4)$$

where X is a discrete-time series ($X = \{x_1, x_2, x_3, \dots, x_n\}$), Y is the time series of delaying τ of X ($Y = \{x_{1+\tau}, x_{2+\tau}, \dots, x_{n-\tau+1}\}$).

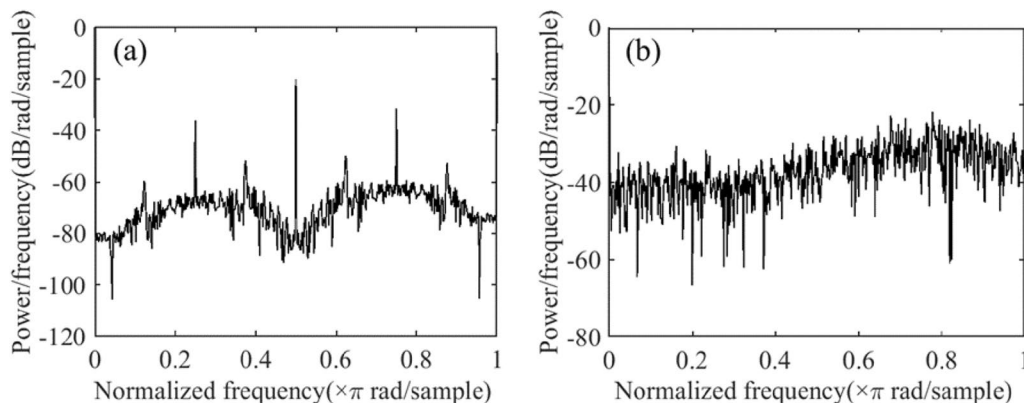


Figure 8 Power spectrum diagram of periodic and chaotic systems: (a) Periodic system, (b) Chaotic system

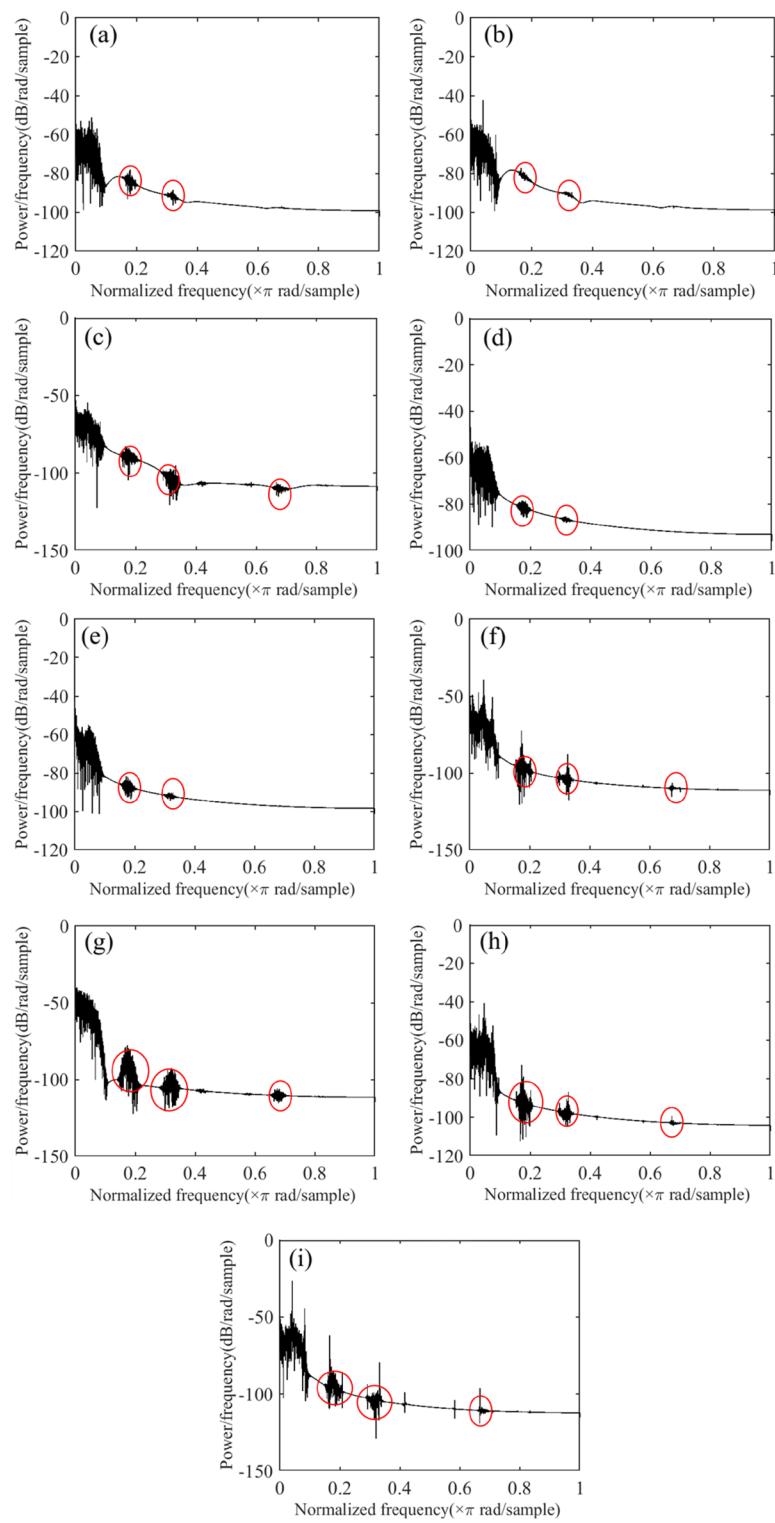


Figure 9 Burnishing friction coefficient power spectra: (a) Test 1, (b) Test 2, (c) Test 3, (d) Test 4, (e) Test 5, (f) Test 6, (g) Test 7, (h) Test 8, (i) Test 9

Table 5 Time delays and optimal embedding dimensions of friction coefficient signals in all tests

Test	1	2	3	4	5	6	7	8	9
Time delay τ	22	25	26	22	22	23	28	25	14
Embedding dimension m	6	5	5	6	6	6	6	7	5

$x_{3+\tau}, \dots, x_{n+\tau}\}$, and $P_{xy}(x_i, y)$ is the joint distribution probability at $X=x_i, Y=y$. $P_X(x_i)$ and $P_Y(y_j)$ are the edge distribution probabilities.

$$\left[\frac{R_{m+1}^2(i, r) - R_m^2(i, r)}{R_m^2(i, r)} \right]^{\frac{1}{2}} = \frac{|X_i - X_i^r|}{R_m(i, r)} > R_{tol}, i = 1, 2, \dots, N, \quad (5)$$

where R_m is the distance between any two points in m -dimensional phase space, R_{m+1} is the distance between any two points in the $(m+1)$ -dimensional phase space, Y_i is a point in the m -dimensional phase space, Y_i^r is the nearest neighbor of Y_i , $r = 1$, and R_{tol} is the threshold value, with $R_{tol} \in [10, 50]$. The values of time delay τ and optimal embedding dimension m for all the experiments are listed in Table 5.

The Lyapunov exponent refers to the average rate of change in two trajectories close to each other in the phase space and separated or aggregated exponentially over time. A chaotic system has an initial value sensitivity; that is, for two very close initial values, the state values are separated at a rapid speed through multiple iterations. Therefore, the Lyapunov exponent λ can be used to determine whether the burnishing system is chaotic [26]. A system with chaotic characteristics can be analyzed by calculating whether the maximum Lyapunov exponent λ is greater than zero [27]. When $\lambda > 0$, the system is chaotic; when $\lambda = 0$, the system is periodic; when $\lambda < 0$, the system will eventually tend to a fixed point.

In this study, the small-data volume method [28] was used to calculate the maximum Lyapunov exponent λ of the friction coefficient with 21,000 points collected from each test group. The calculation formula is expressed as follows:

$$y(i) = \frac{1}{q \times \Delta t} \sum_{j=1}^q \ln d_j(i), \quad (6)$$

where $d_j(i)$ is the distance between each point x_i in the phase space and its closest point x_j after i discrete time steps, Δt is the sampling interval of the friction coefficient time series, and q is the number of non-zero $d_j(i)$. The slope of the curve, $i - y(i)$, calculated using the least-squares method in the region with good linearity, is the maximum Lyapunov λ . The maximum Lyapunov λ values of the friction coefficient signals in all tests are listed in

Table 6 Maximum Lyapunov exponents λ for Test 1–9

Test	Maximum Lyapunov exponent, λ
1	0.1512
2	0.0931
3	0.0232
4	0.0805
5	0.0108
6	0.5492
7	0.0169
8	0.5790
9	0.4305

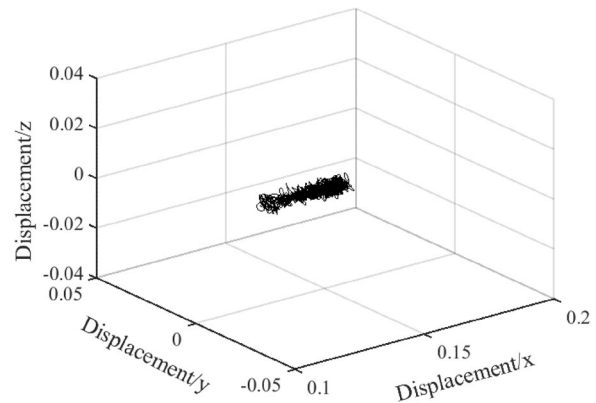
**Figure 10** Phase trajectory of Test 5

Table 6. It can be observed that the maximum Lyapunov λ in each test exceeds zero.

The power spectrum method was used to verify that the burnishing friction coefficient exhibited nonlinear characteristics, and it was preliminarily determined that the burnishing system exhibited chaotic characteristics. Furthermore, if the maximum Lyapunov exponent of the burnishing friction coefficient exceeds zero, the burnishing system is verified to show chaotic characteristics.

Because the burnishing system exhibits chaotic characteristics, based on the variation in the burnishing

friction coefficient with time, its phase trajectory in the three-dimensional space converges in a small area. Test 5 is taken as an example, and the phase trajectory of the burnishing friction coefficient in the three-dimensional space is shown in Figure 10. The phase trajectories stabilize in a small region, and the phase trajectories overlap but never intersect in the three-dimensional space.

4.3 Relationship Between Correlation Dimension and Surface Roughness

The correlation dimension is a parameter that describes the positional relationship of phase points in phase space. The larger the correlation dimension, the more concentrated the phase points, the more stable the system, and the smoother the corresponding machined surface [29]. Based on the G-P algorithm proposed by Grassberger and Procaccia[30–32], the correlation dimension D is defined as follows :

$$C(r) = \frac{1}{N(N-1)} \sum_{i=1}^N \sum_{j=1, j \neq i}^N H(r - \|Y_i - Y_j\|), \quad (7)$$

$$D = \lim_{r \rightarrow \infty} \frac{\ln C(r)}{\ln r}, \quad (8)$$

where $C(r)$ is the correlation integral function, r is a small scalar, $Y_i = \{x_i, x_{i+\tau}, \dots, x_{i+(m-1)\tau}\}$, $i = 1, 2, \dots, N$, $N = n - (m-1)\tau$, n is the count of x_i , $H(\cdot)$ is Heaviside step function. When the value in the brackets is greater than zero, $H(\cdot) = 1$; when the value in the brackets is less than zero, $H(\cdot) = 0$. D is the correlation dimension. When calculating correlation dimension D , the part with better linearity of the $\ln r - \ln C(r)$ curve is selected and fitted linearly using the least-squares method. The slope of the fitting line represents the value of the correlation dimension D of the time series $\{x_1, x_2, \dots, x_n\}$.

For the time series of the friction coefficient signals in all tests, 21000 points were selected for each test to calculate the correlation dimension. The $\ln r - \ln C(r)$ curves are shown in Figure 11. Although the processing parameters are different, the variations in their curves are similar, starting from the first point and finally tending to zero. The selection of the scale-free interval significantly influences the correlation dimension D . Here, the better linearity part is selected using the visual recognition method, shown as the interval between two green lines in Figure 10. Next, the slope value, which represents the correlation dimension D , were calculated (Table 7). It should be noted that the size of the attractor correlation

Table 7 Correlation dimensions and surface roughness values for Test 1–9

Test	Surface roughness S_q (nm)	Correlation dimension D
1	205	4.239
2	297	3.9617
3	319	3.8956
4	151	4.5745
5	156	4.5385
6	133	4.6446
7	131	4.6624
8	78	4.9103
9	92	4.7751

dimension is not necessarily related to the magnitude of the burnishing friction coefficient. This is because the correlation dimension mainly reflects the stability of the system, and the stability or fluctuation of the system state is not necessarily related to the magnitude of the burnishing friction coefficient.

The variation laws between the surface roughness values of the burnished samples and the correlation dimensions of the friction coefficient signals during burnishing are shown in Figure 12, where the blue part indicates the roughness error band. The correlation dimension D in Test 3 was the smallest, but its surface roughness value was the largest. In contrast, the correlation dimension D in Test 8 was the largest, but its surface roughness was the smallest. The overall roughness levels of Tests 1–3 were lower than those of Tests 4–6, and the overall roughness levels of Tests 4–6 were lower than those of Tests 7–9. The corresponding correlation dimensions exhibited the opposite variation law. When the correlation dimension curve exhibited a downward trend, the roughness curve exhibited an upward trend. Thus, the variation trend of the sample surface roughness is opposite to that of the correlation dimension.

The conclusions were further verified using Test 10. Test 10 parameters were obtained from the analysis of the orthogonal experimental table using a surface roughness value of 72 nm and a correlation dimension D of 5.1075. The roughness was lower than that in Test 3, and the correlation dimension D was higher than in Test 3. Therefore, the larger the correlation dimension, the lower the surface roughness value, and the higher the surface smoothness value. The variations in the friction coefficient with the burnishing duration for Test10, the three-dimensional topography, and the $\ln r - \ln C(r)$ curve are shown in Figure 13.

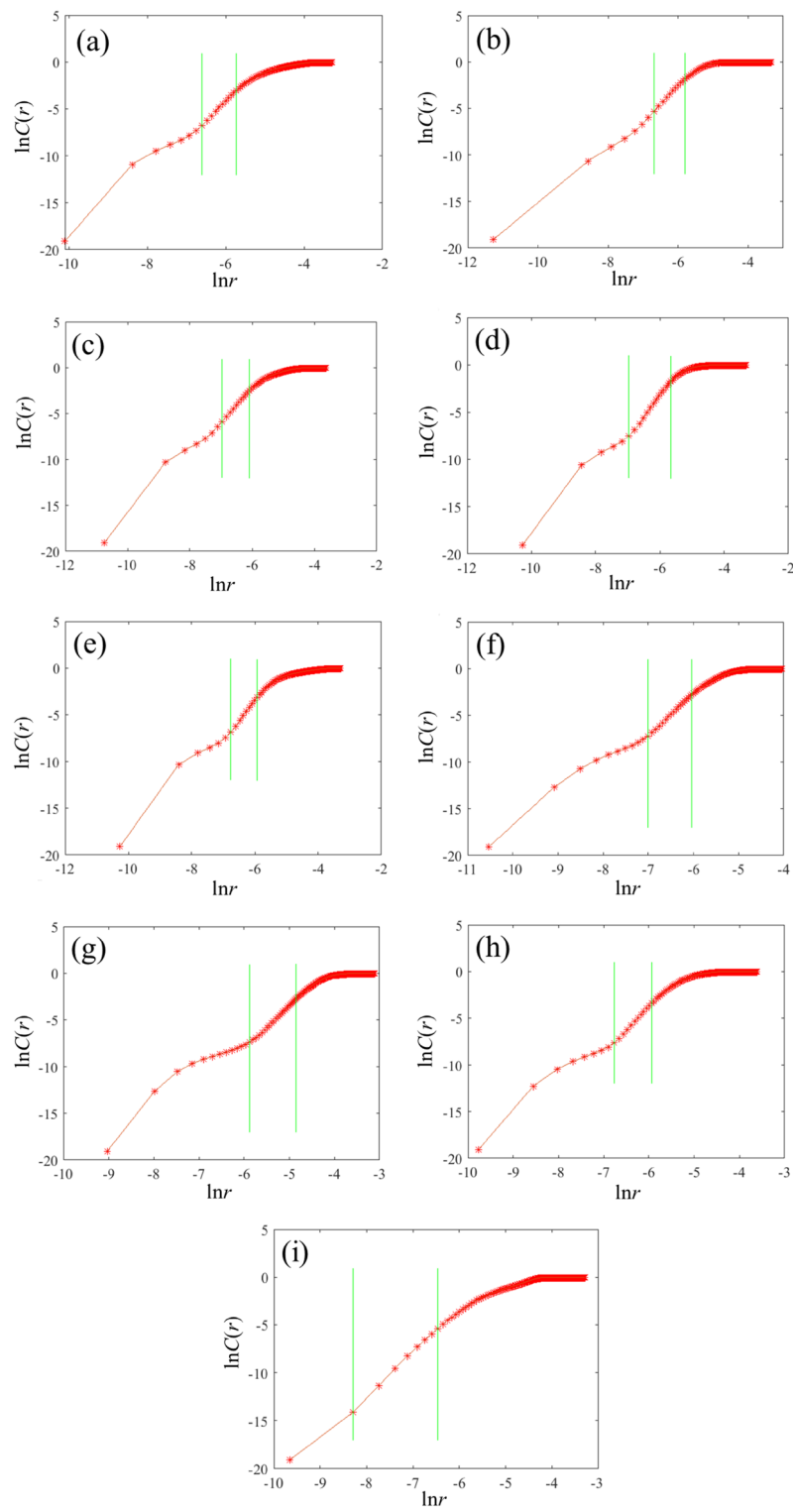


Figure 11 $\ln r$ - $\ln C(r)$: (a) Test 1, (b) Test 2, (c) Test 3, (d) Test 4, (e) Test 5, (f) Test 6, (g) Test 7, (h) Test 8, and (i) Test 9

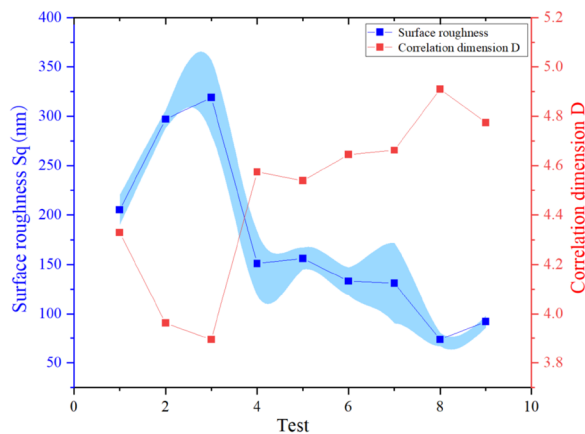


Figure 12 Variation law between correlation dimension and surface roughness

5 Conclusions

- (1) Based on the analysis of the surface roughness variation in the orthogonal experiments, the best surface roughness can be obtained using a 0.06 mm burnishing depth, 3000 r/min spindle speed, and 70 mm/min feed rate. This conclusion was verified by Test 10. The most significant factor influencing the surface roughness was the burnishing depth, followed by the feed rate, and finally, the spindle speed.
- (2) For the aluminum alloy burnishing system, the nonlinear characteristics of the friction coefficient were analyzed qualitatively and quantitatively using the power spectrum and the maximum Lyapunov exponent. The results showed that the friction coefficient had a continuous, broadband power spectrum and a positive Lyapunov exponent. The burnishing friction coefficient exhibits chaotic characteristics, demonstrating that the burnishing system is a chaotic system.
- (3) By investigating the relationship between the surface roughness of the burnished samples and the correlation dimension of the friction coefficient, the variation trend of the correlation dimension was found to be opposite to that of the surface roughness. The larger the correlation dimension, the lower the surface roughness value, and the higher the surface quality, which was further verified using Test 10.

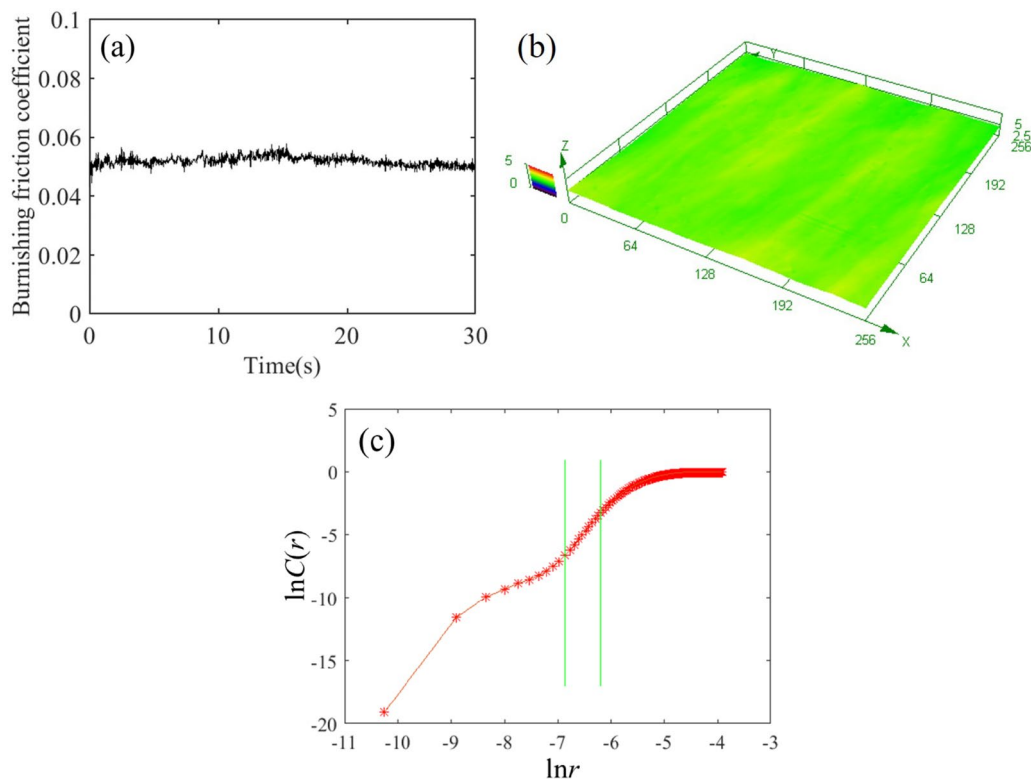


Figure 13 (a) Variation in burnishing friction coefficient with burnishing duration for Test 10, (b) three-dimensional topography, and (c) the curve of $\ln r - \ln C(r)$ curve

- (4) The friction coefficient can be extracted from the burnishing process in real time, and the correlation dimension can be calculated on-line. Therefore, the evolution of the correlation dimension with the burnishing process can be used to evaluate the surface roughness of the burnished sample online. This aspect has essential application prospects in achieving on-line monitoring of burnishing quality.

Acknowledgments

The authors sincerely thank Professor Mingxue Shen of East China Jiaotong University for his assistance during manuscript preparation.

Author Contributions

Zhongyu Piao and Cong Ding was in charge of the whole trial; Zhipeng Yuan wrote the manuscript; Zhenyu Zhou conducted the experiments; Zhiguo Jiang and Zeyu Zhao conceived and designed the research. All authors read and approved the final manuscript.

Authors' Information

Zhipeng Yuan, born in 1996, is currently a master candidate at Key Laboratory of Special Purpose Equipment and Advanced Processing Technology (Zhejiang University of Technology), Ministry of Education, China.

Zhenyu Zhou, born in 1993, is currently a Ph.D. candidate at Key Laboratory of Special Purpose Equipment and Advanced Processing Technology (Zhejiang University of Technology), Ministry of Education, China. He received his bachelor's degree from Zhejiang University of Technology, China, in 2016. His research interests include surface engineering.

Zhiguo Jiang, born in 1997, is currently a Ph.D. candidate at Key Laboratory of Special Purpose Equipment and Advanced Processing Technology (Zhejiang University of Technology), Ministry of Education, China.

Zeyu Zhao, born in 1997, is currently a master candidate at Key Laboratory of Special Purpose Equipment and Advanced Processing Technology (Zhejiang University of Technology), Ministry of Education, China.

Cong Ding, born in 1990, is currently an associate professor at School of Mechanical Engineering, Zhejiang University of Technology, China. She received her bachelor's degree from China University of Mining and Technology in 2014 and PhD degree from China University of Mining and Technology, in 2019. Her research interests include surface engineering and tribology.

Zhongyu Piao, born in 1982, is currently an associate professor in the School of Mechanical Engineering, Zhejiang University of Technology, China. His research interests include surface engineering and tribology.

Funding

Supported by National Natural Science Foundation of China (Grant Nos. 52175194, 52105215, 52075047), Zhejiang Provincial Natural Science Foundation of China (LR23E050002), Fundamental Research Funds for the Provincial Universities of Zhejiang (Grant No. RF-A2019008), Key Laboratory of E&M (Zhejiang University of Technology), Ministry of Education & Zhejiang Province (Grant No. EM2021120103).

Availability of data and materials

All data, models, and materials generated or used during the study appear in the submitted article.

Competing interests

The authors declare no competing financial interests.

Received: 7 December 2021 Revised: 31 August 2022 Accepted: 18 December 2022

Published online: 05 January 2023

References

- [1] B T Zhou, X F Wei, Y B Wang, et al. Effect of lanthanum addition on microstructures and corrosion behavior of ZnAl-LDHs film of 6061 aluminum alloys. *Surface & Coatings Technology*, 2019, 379: 125056.
- [2] B Zhou, B Liu, S Zhang, et al. Microstructure evolution of recycled 7075 aluminum alloy and its mechanical and corrosion properties. *Journal of Alloys and Compounds*, 2021, 879: 160407.
- [3] E N Kablov, V V Antipov, J S Oglodkova, et al. Development and application prospects of aluminum-lithium alloys in aircraft and space technology. *Metallurgist*, 2021, 65(1-2): 72-81.
- [4] W Xiao, Y Wang. Corrosion resistance of aluminum fluoride modified 6061 aluminum alloy. *Materials Letters*, 2021, 298: 129932.
- [5] J Oh, H D Park, M Gwak, et al. Mechanical property enhancement in gradient structured aluminum alloy by ultrasonic nanocrystalline surface modification. *Mat. Sci. Eng. A-Struct.*, 2021, 812: 141101.
- [6] X C Xu, D X Liu, X H Zhang, et al. Effects of ultrasonic surface rolling on the localized corrosion behavior of 7B50-T7751 aluminum alloy. *Materials (Basel)*, 2020, 13(3): 738.
- [7] C Chen, F R Chen, H J Zhang. Surface nanocrystallization of 7A52 aluminum alloy welded joint by aging and ultrasonic impact compound treatment. *Rare Metal Materials and Engineering*, 2018, 47(9): 2637-2641.
- [8] L H Zhu, Y J Guan, Z S Wang, et al. Influence of surface nanocrystallization and partial amorphization induced by ultrasonic shot peening on surface properties of 7075 aluminum alloy. *Journal of Materials Engineering and Performance*, 2020, 29(11): 7693-7709.
- [9] T Gao, Z D Sun, H Q Xue, et al. Effect of surface mechanical attrition treatment on high cycle and very high cycle fatigue of a 7075-T6 aluminum alloy. *International Journal of Fatigue*, 2020, 139: 105798.
- [10] Z R He, Y Z Shen, J Tao, et al. Laser shock peening regulating aluminum alloy surface residual stresses for enhancing the mechanical properties: Roles of shock number and energy. *Surface & Coatings Technology*, 2021, 421: 127481.
- [11] G Z Ma, B S Xu, H D Wang, et al. Research on the microstructure and space tribology properties of electric-brush plated Ni/MoS₂-C composite coating. *Surface and Coatings Technology*, 2013, 221: 142-149.
- [12] S Y Chen, G Z Ma, H D Wang, et al. Evaluation of adhesion strength between amorphous splat and substrate by micro scratch method. *Surface & Coatings Technology*, 2018, 344: 43-51.
- [13] P F He, G Z Ma, H D Wang, et al. Tribological behaviors of internal plasma sprayed TiO₂-based ceramic coating on engine cylinder under lubricated conditions. *Tribology International*, 2016, 102: 407-418.
- [14] H Ma, G L Qin, Z Y Dang, et al. Interfacial microstructure and property of 6061 aluminium alloy/stainless steel hybrid inertia friction welded joint with different steel surface roughness. *Materials Characterization*, 2021, 179: 111347.
- [15] Z Y Zhou, Q Y Zheng, C Ding, et al. Research on the promotion mechanism of surface burnishing process by two-dimensional ultrasonic vibration. *Journal of Materials Research and Technology*, 2021, 13: 1068-1082.
- [16] Z Y Zhou, Q Y Zheng, C Ding, et al. Investigation of two-dimensional ultrasonic surface burnishing process on 7075-T6 aluminum. *Chinese Journal of Mechanical Engineering*, 2021, 34(1): 19.
- [17] Z Y Zhou, Q Y Zheng, C Ding, et al. Effect of surface burnishing process with different strain paths on the copper microstructure. *Journal of Manufacturing Processes*. 2021;71:653-668.
- [18] A Leon, E Aghion. Effect of surface roughness on corrosion fatigue performance of AlSi10Mg alloy produced by selective laser melting (SLM). *Materials Characterization*, 2017, 131: 188-194.
- [19] Z Y Zhao, S B Wang, Z H Wang, et al. Surface roughness stabilization method based on digital twin-driven machining parameters self-adaption adjustment: a case study in five-axis machining. *Journal of Intelligent Manufacturing*, 2022, 33(4): 943-952.
- [20] J T Xiao, P F Ju, X S Zang, et al. Preparation and performance analysis of lubricating and corrosion-resistant composite coating on aluminum alloy surface. *China Surface Engineering*, 2021, 34(4): 38-45.(in Chinese)
- [21] C Ding, Z Y Zhou, Z Y Piao. Investigation on the running-in quality at different rotating speeds by chaos theory. *International Journal of Bifurcation and Chaos*. 2021, 31(7): 2150108.

- [22] S R Ge, H Zhu. Chaotic characteristics of tribological systems. *Journal of Mechanical Engineering*, 2004, 40(12): 10-13. (in Chinese)
- [23] F Takens. The reconstruction theorem for endomorphisms. *Bulletin Brazilian Mathematical Society*, 2002, 33(2): 231-262.
- [24] S H Lang, H Zhu, S Z You. Vector characterization and evolution of the running-in attractor. *Tribology International*, 2021, 157: 106888.
- [25] M B Kennel, R Brown, H D Abarbanel. Determining embedding dimension for phase-space reconstruction using a geometrical construction. *Phys Rev A*, 1992, 45(6): 3403-3411.
- [26] N V Kuznetsov, T A Alexeeva, G A Leonov. Invariance of Lyapunov exponents and Lyapunov dimension for regular and irregular linearizations. *Nonlinear Dynamics*, 2016, 85(1): 195-201.
- [27] A Wolf, J B Swift, H L Swinney, et al. Determining Lyapunov exponents from a time series. *Physica D: Nonlinear Phenomena*, 1985, 16(3): 285-317.
- [28] M T Rosenstein, J J Collins, C J De Luca. A practical method for calculating largest lyapunov exponents from small data sets. *Physica D-Nonlinear Phenomena*, 1993, 65(1-2): 117-134.
- [29] C Ding, H Zhu, G D Sun, et al. Effects of system parameters on the chaotic properties of 52100 steel sliding against 5120 steel. *Wear*, 2019, 420: 68-78.
- [30] A Ben-Mizrachi, I Procaccia, P Grassberger. Characterization of experimental (noisy) strange attractors. *Physical Review A*, 1984, 29(2): 975-977.
- [31] C X Luo, S X Jing, X M Han, et al. Fluid-solid coupling field analysis of centrifugal fan based on nonlinear dynamics. *Journal of Vibroengineering*, 2017, 19(7): 5473-5481.
- [32] X Z Wu, Y Sun, Y Wang, et al. Correlation dimension and bifurcation analysis for the planar slider-crank mechanism with multiple clearance joints. *Multibody System Dynamics*, 2021, 52(1): 95-116.

Submit your manuscript to a SpringerOpen[®] journal and benefit from:

- Convenient online submission
- Rigorous peer review
- Open access: articles freely available online
- High visibility within the field
- Retaining the copyright to your article

Submit your next manuscript at ► [springeropen.com](https://www.springeropen.com)